# Making GAN-Generated Images Difficult To Spot: A New Attack Against Synthetic Image Detectors

Xinwei Zhao

xz355@drexel.edu

Matthew C. Stamm

mstamm@drexel.edu

#### **Abstract**

Visually realistic GAN-generated images have recently emerged as an important misinformation threat. Research has shown that these synthetic images contain forensic traces that are readily identifiable by forensic detectors. Unfortunately, these detectors are built upon neural networks, which are vulnerable to recently developed adversarial attacks. In this paper, we propose a new anti-forensic attack capable of fooling GAN-generated image detectors. Our attack uses an adversarially trained generator to synthesize traces that these detectors associate with real images. Furthermore, we propose a technique to train our attack so that it can achieve transferability, i.e. it can fool unknown CNNs that it was not explicitly trained against. We demonstrate the performance of our attack through an extensive set of experiments, where we show that our attack can fool eight state-of-the-art detection CNNs with synthetic images created using seven different GANs.

# 1. Introduction

Recent technological advances have enabled the creation of synthetic images that are visually realistic. Generative adversarial networks (GANs) [17] in particular have driven this development. Several GANs have been proposed that are capable of synthetically generating images of both objects and human faces that are convincingly real to human observers [12, 25, 24, 6, 38, 23, 10]. Unfortunately, these synthetic image generation techniques can be used for malicious purposes, such as the creation of fake personas to be used as part of misinformation campaigns.

To combat this threat, researchers have developed a variety of techniques to detect GAN-generated images [15, 34, 36, 46, 41] and to attribute them to the specific GAN used to create them [32, 33, 43]. At the same time, adversarial examples have arisen as a new threat to classifiers built from neural networks [39, 18, 27, 37, 8, 30]. These represent important threats to the forensic community because they can be used as an anti-forensic attack against forensic detectors [2, 7, 19]. Recent work from the forensic community,

however, suggests that these attacks may not achieve transferability, i.e. they may be unable to attack classifiers other than those that they were directly trained against [1, 47].

For an anti-forensic attack to be successful, it must (1) fool a victim classifier and (2) maintain high visual quality within the attacked image. Furthermore, it is highly desirable for an attack to (3) transfer to victim classifiers not seen during training and (4) be easily deployable in practical scenarios, i.e. it should work on images of any size, not require specific knowledge of the image window analyzed by a forensic CNN, deploy quickly and efficiently, etc.

In this paper, we propose a new attack that is capable of fooling forensic synthetic image detectors into thinking that GAN-generated images are in fact real images. This attack achieves each of the four goals described above, including a significant degree of transferability, which enables it to attack victim classifiers that are unseen during training. Instead of crafting adversarial examples that exploit flaws in forensic deetctors, our attack uses an anti-forensic generator to synthesize forensic traces associated with real images. We propose GAN-based approaches for training our anti-forensic generator for both white box scenarios as well as zero-knowledge scenarios. Once the anti-forensic generator is trained, it can be used to attack images of arbitrary size without requiring re-training or additional tuning to the image under attack.

The main contributions of this work are as follows:

- We demonstrate that an anti-forensic generative attack can be used to fool forensic CNNs designed to detect GAN-generated images.
- We propose a new anti-forensic generator that is able to synthesize forensic traces associated with real images while introducing no perceptible distortions into an attacked image. We show that our proposed generator achieves in a higher attack success rate and image quality than other existing anti-forensic generators.
- We propose an ensemble loss training strategy that enables our attack to achieve transferability in zeroknowledge scenarios.
- We demonstrate the effectiveness of our attack against many state-of-the-art forensic CNNs, using a synthetic

images from a wide variety of different GANs.

#### 2. Related Work

Here we briefly review related work on detecting GANgenerated images and adversarial attacks.

GAN-Generated Image Detectors: To defend against the misinformation threat posed by synthetic media, significant research has been done to create GAN-generated image detection algorithms [43, 31, 15, 34, 36, 46, 41]. Previous research has shown that GANs leave behind forensic traces that are distinguishable from real images. These forensic traces left by GANs can be utilized to detect GAN-generated images. Some approaches operate in a data driven manner [31, 41, 15], while other approaches utilize semantic information [34] or hand-crafted features [36]. Additionally, forensic techniques are also developed to identify which GAN was used to generate an image [32, 43, 46].

Adversarial Attacks on Forensic Classifiers: At the same time, adversarial attacks on neural networks have emerged as an important threat [18, 44]. These attacks can be adapted to attack forensic classifiers [2]. Roughly speaking, we can group these attacks into two different families: adversarial-example-based attacks and GAN-based attacks.

Attacks based on adversarial examples operate by creating perturbations that are added to an image. These perturbations cause a victim classifier to misclassify the image. Several techniques have been proposed to create these perturbations, including L-BFGS [39], FGSM and iterative-FG [18, 27], JSMA [37], CW [8], PGD [30]. Attacks based on adversarial examples have been used to forensic algorithms, including camera model identification algorithms [19] and deepfake detectors [7]. Research by Barni et. al has shown, however, that adversarial example attacks do not transfer well to other forensic classifiers [1].

Previous research has also shown that GANs can be utilized to construct attacks that falsify forensic traces. GANs were used by Chen et al. to falsify camera model fingerprints [9] and by Cozzolino et al. to falsify device fingerprints [14]. Kim et. al used a GAN to remove forensic traces left by median filtering [26]. However, research has shown that the GAN-based anti-forensic attacks also have trouble achieving transsferability [47].

# 3. Proposed Attack

#### 3.1. Overivew

Our attack is designed to modify a GAN-generated image I so that a forensic CNN will instead classify it as a 'real' image. This forensic CNN is alternately referred to as the victim classifier, and is trained to differentiate between real and GAN-generated images.

Our attack operates by passing the GAN-generated im-

age through a pre-trained anti-forensic generator G in order to falsify its forensic traces. The anti-forensic generator is designed to remove forensic traces associated with GAN-generated images and synthesize traces associated with 'real' images. As a result, a victim classifier will classify the attacked GAN-generated image G(I) as a real one. Furthermore, the anti-forensic generator designed to make no changes to the image's contents and to introduce no visually perceptible distortions into the attacked image. This will prevent a human from visually identifying that an image was attacked.

The anti-forensic generator in our attack learns to synthesize 'real' forensic traces through adversarial training. It is trained as part of a GAN in which the discriminator is replaced by a forensic classifier (or set of classifiers) that has been pre-trained to learn the distribution of forensic features associated with real and GAN-generated images.

Different strategies are used to train the anti-forensic generator depending on whether the attack is launched in a white box or zero-knowledge scenario. In the white box scenario, our attack aims to synthesize forensic features with the distribution learned by the victim classifier, even if they deviate from the ideal feature distribution of real images. In the zero-knowledge scenario, our attack aims to learn the distribution of forensic features of real images. However it avoids synthesizing features in regions where different classifiers may make different decisions. Instead, it aims to synthesize features that any classifier will likely associate with a real image.

We note that once our anti-forensic generator is trained, our attack can be launched against any image without retraining. Furthermore, since our attack is based on a convolutional generator, we can attack images of any size without the need to modify our generator or attack structure. This differs from adversarial example generation techniques, which iteratively learn unique perturbations for each image that are the same size as the victim classifier's input.

# 3.2. Difference From Adversarial Examples

Our proposed attack is different from adversarial example generation algorithms in several ways. Most importantly, our attack operates using a fundamentally different approach than adversarial examples. Adversarial examples aim to exploit non-ideal properties neural networks that can cause them to misclassify an input image. Several explanations have been posited for the non-ideal properties of neural networks that adversarial examples exploit, such as imperfections caused by the locally-linear nature of neural networks [18] or that there is misalignment between the features used by humans and those learned by neural networks when performing the same classification task [22].

By contrast, our attack does not intend to exploit nonideal properties of the classifier. Instead, our attack aims to accurately synthesize the forensic features that a neural network would *correctly* use to classify an unattacked image. We are able to do this because forensic traces are typically not visible to the human eye. As a result, we can completely falsify these traces without modifying the contents of an image. This approach may not translate well to attacks on classifiers for vision, because ideally the features learned by these classifier should correspond to visible attributes of an image. We believe that attempting to accurately synthesize 'real' forensic features is the key to the transferability of our attack in zero-knowledge scenarios.

Additionally, adversarial example generation algorithms operate by creating perturbations that are added to an image in order to fool a classifier. These perturbations are the same size as the input to the victim classifier. They are learned through an iterative process in which an intermediate version of the attacked image is presented to the victim classifier, gradient information is inferred, and the attack perturbation is updated. As a result, a new perturbation must be iteratively learned for each image under attack.

By contrast our attack learns a convolutional generator which is trained in advance. The generator is not modified or customized to the image under attack. As a result, any image of arbitrary size can be passed through the generator, not just images with the same size as the victim CNN's input. Additionally, our attack can be quickly deployed since it does not require iterative training for each new image.

# 3.3. Proposed Anti-Forensic Generator

The proposed anti-forensic generator consists of a sequence of convolutional layers followed by ReLU activations [35] shown in Figure 1. The first three convolutional layers use 64 filters, the middle three convolutional layers use 128 filters, and the final convolutional layer uses three filters to reduce the 128 feature maps to a three color channel image. The output of the generator is the summation of the input of the generator and the output of the last activated convolutional layer. The skip connection is designed to give the generator a better initialization for producing high visual quality attacked images. All convolutional layers use  $3 \times 3$ filter with stride 1. The small filter size allows the generator to synthesize forensic traces in small areas. We avoid using any pooling layers to ensure that the output of the generator is of the same size as the input of the generator. Therefore, the proposed anti-forensic generator can be applied to images of arbitrary sizes, and does not need to be trained for images of different sizes individually. This characteristic makes the deployment of the proposed anti-forensic generator efficient and quick.

We note that our proposed generator is intentionally lightweight. This allows it to be trained using widely available commercial GPUs. This also enables it to be quickly deployed at attack time.

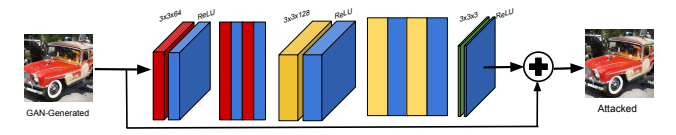


Figure 1. Architecture of the proposed anti-forensic generator.

#### 3.4. Anti-Forensic Generator Training

When adversarially training the anti-forensic generator G, we use a loss function formulated to ensure that an attacked image can both fool a victim classifier and maintain high visual quality. This loss function  $\mathcal{L}_G$  consists of the weighted sum of two terms: the perceptual loss  $\mathcal{L}_p$  and classification loss  $\mathcal{L}_c$ , such that

$$\mathcal{L}_G = \alpha \mathcal{L}_p + \mathcal{L}_c, \tag{1}$$

where  $\alpha$  is used to balance the trade-off between the visual quality and performance of the attack.

**Perceptual Loss:** This term is used to minimize distortions introduced by the anti-forensic generator and control the visual quality of the attacked image. We define this term as the mean absolute difference between the GAN-generated image I (i.e the input of the generator ) and the attacked image produced by the generator G(I), such that

$$\mathcal{L}_p = \frac{1}{N} \|I - G(I)\|_1, \tag{2}$$

where N is the number of pixels in I and G(I)

Classification Loss: This term is used to measure if the attacked images produced by the anti-forensic generator can fool the CNN detector used for training. It allows the generator to learn forensic traces learned by the CNN detectors. For the white-box attack, the classification loss is provided by the victim classifier. For the zero knowledge attack, the classification loss is provided by an ensemble of classifiers chosen by the attack.

#### 3.5. White-Box Attack Training

In the white-box scenario, the attacker has direct access to the forensic CNN under attack. As a result, the anti-forensic generator can be directly trained against the victim classifier. In this case, we define the classification loss  $\mathcal{L}_c$  as the softmax cross-entropy between the CNN detector's output of attacked images and the real class. Specifically,

$$\mathcal{L}_c = -\sum_{k=1}^2 t_k \log \left( C(G(I))_k \right), \tag{3}$$

where  $C(\cdot)$  is the victim classifier and  $t_k$  is the  $k^{th}$  entry of ideal softmax vector with a 1 for the real class and a 0 for the fake class. Defining the classification loss in this manner incentivizes the anti-forensic generator to learn the victim classifier's model of forensic features from real images.

#### 3.6. Zero Knowledge Attack Training

In the zero knowledge scenario, the attacker has no access to the victim classifier that they wish to attack, nor do they know its architecture. This differs from the black box scenario in which the attacker can probe the victim classifier through an API, then observe the victim classifier's input-output relationship. Instead, the attacker must rely entirely on the transferability of their attack to fool the victim CNN.

To achieve transferability, we propose adversarially training against an ensemble of forensic classifiers created by the attacker. Here, the classification loss  $\mathcal{L}_c$  is formulated as the weights sum of individual classification loss pertaining to each CNN detector in the ensemble,

$$\mathcal{L}_c = \sum_{s=1}^{S} \beta^{(s)} \mathcal{L}_c^{(s)} \tag{4}$$

where S is the number of CNN detectors in the ensemble,  $\mathcal{L}_c^{(s)}$  corresponds to individual classification loss of the  $s^{th}$  CNN detector calculated using Equation 3,  $\beta^{(s)}$  corresponds to the weight of  $s^{th}$  individual classification loss.

Each classifier in the ensemble learns to partition the forensic feature space into separate regions for real and GAN-generated images. By defining the classifier loss in this fashion, we incentivize the anti-forensic generator to synthesize forensic features that lie in the intersection of these regions. If a diverse set of classifiers are used to form the ensemble, this intersection will likely lie inside the decision region that other classifiers associate with real images.

We note that this approach differs from adversarially training against an ensemble classifier. An ensemble classifier fuses the decisions of several weak classifiers to form an accurate representation of the ideal classification boundary separating real from GAN-generated images. We wish to avoid generating features in regions near the ideal decision boundary, since many different classifiers will likely make different decision in this region. By synthesizing features that *all* classifiers in our ensemble agree are real, we move away from the ambiguous region near the ideal decision boundary and further into the space that likely corresponds to real images.

#### 4. Experimental Setup

In this section, we provide details of the experimental evaluation of our proposed attack, including the datasets used in our experiments, the baseline performance of the forensic CNNs we attacked, and the procedure used to evaluate our white box and zero-knowledge attack.

#### 4.1. Datasets

We created two datasets to evaluate our attacks, each containing both real and GAN-generated images. The first dataset contains only images of human faces, while the second contains images of non-human objects.

Human Face Dataset: This dataset consists of real images and GAN-generated images of human faces. The GAN-generated images were created using StyleGAN [24], StyleGAN2 [25], and StarGAN-v2 [12]. StyleGAN and StyleGAN2 generated images were downloaded from publicly available datasets shared by Nvidia Research Lab [28, 29]. The StarGAN-v2 generated images were created using pre-trained StarGAN-v2 generator shared at [11]. The real images were downloaded from FFHQ dataset [25] and CelebA-HQ dataset [23]. In total, the human face dataset contains 66,000 real images with 44,000 from FFHQ and 22,000 from CelebA-HQ; 126,000 GAN-generated images, 42,000 using StyleGAN, 42,000 using StyleGAN2, and 42,000 using StarGAN-v2. The size of all StyleGAN and StyleGAN2 generated images, as well as the real images from the FFHQ and Celeb-A are all  $1024 \times 1024$  pixels. The size of StarGAN-v2 generated images are  $256 \times 256$ .

Next, we partitioned the data into two disjoint training sets, the *D-set* and the *A-set*, as well as an evaluation set *Eval-set*. The *D-set* was used to train the victim forensic CNN detectors. It contains 60,000 GAN-generated images drawn equally from StyleGAN, StyleGAN2 and StarGAN-v2; and 60,000 real images with 40,000 from FFHQ and 20,000 from CelebA-HQ. The *A-set* was used to train the proposed attack. Since training the proposed attack only requires GAN-generated images, *A-set* contains 60,000 GAN-generated images drawn equally from Style-GAN, StyleGAN2 and StarGAN-v2.

To demonstrate the effectiveness of the proposed attack, we benchmarked the baseline performance of the victim forensic CNN detectors and evaluated the performance of our proposed attack against these CNNs using a common evaluation set, *Eval-set*. The *Eval-set* contains 6,000 GAN-generated images drawn equally from StyleGAN, Style-GAN2 and StarGAN-v2; and 6,000 real images with 4,000 from FFHQ and 2,000 from CelebA-HQ.

Object Dataset: This dataset contains real images and GAN-generated images of objects. The object dataset is a subset of publicly available ForenSynths dataset [41]. The ForenSynths dataset was created to demonstrate that CNNs could learn general forensic traces of synthesized images. Therefore CNNs trained on generated images produced by one GAN method can detect generated images produced by other generative models. The training set of ForenSynths dataset contains only ProGAN generated images of objects and real images from LSUN dataset [42]. The testing set of ForenSynths dataset contains varying numbers of generated images produced by 12 different generative methods.

From the training set of the ForenSynths dataset, we created two disjoint training sets: *D-set* for training victim CNN detectors and *A-set* for training the proposed at-

Table 1. The number of GAN-generated images in the *Eval-set* of the object dataset.

GANs	ProGAN	CycleGAN	StyleGAN	StyleGAN2	BigGAN	GauGAN
No. of images	4,000	1,300	6,000	8,000	2,000	5,000

tack. *D-set* contains 50,000 randomly selected ProGAN generated images and 50,000 randomly selected real images. Since training the proposed attack only requires GAN-generated images, *A-set* contains 50,000 randomly selected ProGAN generated images.

To demonstrate the effectiveness of the proposed attack, we benchmarked the baseline performance of victim forensic CNN detectors and evaluated the performance of our proposed attack against these CNNs using a common evaluation set, Eval-set. Eval-set contains 4,000 real images from LSUN and all the generated images of objects created by six different GAN methods from the testing set of Foren-Synths dataset. These GAN methods are ProGAN [23], CycleGAN [48], StyleGAN [24], StyleGAN2 [25], Big-GAN [6], and GauGAN [38]. Since the numbers of images generated by each GAN method are different in the ForenSynths dataset, we listed them in Table 1. The object dataset was created to demonstrate the proposed attack can be trained on images generated by one GAN method (ProGAN) and transfer to falsify forensic traces of images generated by other GAN methods (six other GAN methods in Table 1) unseen by the attack.

# 4.2. Victim Forensic CNN Detectors

Before training and evaluating the proposed attack, we trained and benchmarked the performance of forensic CNNs on detecting GAN-generated images. These forensic CNNs were trained as binary classifiers to differetiate between real images and GAN-generated images. To evaluate our proposed attack, we used eight state-of-the-art CNN models trained as GAN-generated image detectors. These CNN models were designed for computer vision, mulitmedia forensics, or steganalysis. They are Xception [13], ResNet-50 [20], DenseNet [21], MISLNet [3], PHNet [5], SRNet [4], Image CNN [45], and CamID CNN [40]. We trained each forensic CNN individually using *D-set* of the human face dataset and the object dataset. This yielded 16 CNN detectors in total and formed the set of victim classifiers we attacked in this paper.

All CNN detectors were trained from scratch for 20 epochs on both datasets. The input size of each CNN was a  $256 \times 256$  image. For images of resolution  $1024 \times 1024$ , we randomly cropped a  $256 \times 256$  pixel patch from each image during training and testing. We chose the set of hyperparameters for each CNN that yielded the highest classification accuracy after a grid search. For Xception the learning rate started at 0.001; for ResNet-50 the learning rate started at 0.0001 and for all other CNNs the learning rate

Table 2. Baseline classification accuracies of the victim CNN detectors achieved on the human face dataset and the object dataset.

CNNs	Human Face Dataset	Object Dataset
Xception	99.67%	99.75%
ResNet-50	78.26%	99.14%
DenseNet	96.39%	97.04%
MISLNet	99.93%	99.15%
PHNet	95.15%	99.73%
SRNet	99.50%	99.78%
Image CNN	99.49%	99.10%
CamID CNN	99.16%	99.46%
Avg.	95.94%	99.14%

started at 0.0005. These learning rates decayed by half every 4 epochs. Weights were initialized using Xavier initializer [16], biases were initialized as 0's, and both were optimized using stochastic gradient descent.

To benchmark the performance of the victim CNN detectors, we calculated the classification accuracy achieved by each CNN detector. The classification accuracy is defined as the percentage of the real and GAN-generated images that were correctly classified by the CNN detector out of all images in *Eval-set*. The classification accuracy achieved by each victim CNN detector on both datasets are shown in Table 2. On average, we achieved 95.94% classification accuracy on the human face dataset and 99.14% classification accuracy on the object dataset. The results showed that the CNN detectors used in this paper were not biased.

#### 4.3. White-Box Attack

The first set of experiments was designed to evaluate the effectiveness of our proposed attack in the white-box scenario. Here, we assume the attacker has access to the victim classifier and can train directly against it.

For each victim CNN detector trained on the human face dataset and the object dataset, we trained an individual antiforensic generator to attack it. To evaluate the performance of the anti-forensic generator, we used the generator to attack each GAN-generated image in the *Eval-set*, saving the attacked images to disk as PNG files. This is to ensure the pixel values of attacked images reside in the range from 0 to 255. Next, we calculated the attack success rate by using the victim CNN detector to classify the attacked images. We also calculated the mean PSNR and mean SSIM between the GAN-generated images and the attacked images to evaluate the visual quality of the attacked images.

The anti-forensic generators presented in this paper were trained from scratch for 32 epochs with a learning rate of 0.0001. Weights were initialized using Xavier initializer [16] and biases were initialized as 0's, and were optimized using stochastic gradient descent. To balance the image quality and attack success rates,  $\alpha$  in equation 1 was chosen after a grid search range from 1 to 200 with an incre-

ment of 20. Specifically,  $\alpha$  was chosen to be 20 for attacks on the human face dataset and 100 for attacks on the object dataset. When training our attack on the human face dataset, we randomly cropped  $256\times256$  patches from images of size  $1024\times1024$ .

Comparing with Other Generators: We compared the performance of the proposed anti-forensic generator with two other generators used in previous GAN-based attacks. Kim et al. used a residual generator adversarially trained to remove median filtering traces [26]. Chen et al. used MIS-LGAN generator trained to falsify forensic traces of camera models. We repeated experiments on both datasets using the residual generator and the MISLGAN generator.

## 4.4. Zero Knowledge Attack

This set of experiments was conducted to evaluate the proposed attack in the zero knowledge scenario. We assume the attacker has no knowledge about the victim CNN detector that the investigator would use to classify images. Particularly, the attacker has no access to the victim CNN detector and cannot observe any input or output of the CNN detector, since the investigator may use a private CNN detector that the attacker by all means cannot have access to. This is a more realistic yet challenging scenario. In the zero-knowledge scenario, we evaluated the transferability of the proposed attack to attack unseen CNN detectors.

To achieve the transferability, we built an ensemble of forensic CNN detectors to train the proposed anti-forensic generator. To mimic the zero knowledge scenario, each ensemble used to train the attack did not include the victim classifier. We assume that if the attacker has no knowledge of the victim classifier's architecture, the attacker will use all available CNNs in their ensemble to strenthen their attack. However, due to limited GPU memory, Xception was always excluded from the training ensemble in our experiments. During training, we used the same hyperparameters and other settings as the white-box scenario.

#### 5. Results and Discussions

In this section, we present and discuss the results achieved on the human face dataset and the object dataset in the white-box scenario and the zero knowledge scenario.

#### 5.1. Results for White-Box Attack

Table 3 shows the performance our attack achieved on the human face dataset, and Table 4 shows performance of our attack on the object dataset. Attack success rates, defined as the percentage of attacked images classified as 'real' images, are shown to the left of the double bar, while image quality measures (mean PSNR and mean SSIM) are shown to the right.

Table 3. Attack success rates and image quality achieved for white

box attacks on the Human Face Dataset.

Xception   1.0000   1.0000   1.0000   1.0000   45.52   0.9875	Proposed Adversarial Generator										
ResNet-50	CNNs	StarGAN-v2	StyleGAN	StyleGAN2	Avg.	M_PSNR	M_SSIM				
DenseNet         0.9385         0.9770         0.9970         0.9708         54.28         0.9997           MISLNet         0.9965         0.9905         0.9950         0.9940         51.28         0.9925           PHNet         1.0000         0.8497         0.9985         0.9494         41.85         0.9753           SRNet         0.8080         0.8855         0.9480         0.8805         50.97         0.9922           ImageCNN         0.9854         0.9935         0.8505         0.9431         53.64         0.9928           Avg.         0.9270         0.9357         0.9471         0.9366         48.95         0.9870           Residual Generator [26]           CNNs         StarGAN-v2         StyleGAN2         Avg.         M.PSNR         M.SSIR           Kception         0.9820         0.9940         0.9770         0.9843         29.01         0.9498           ResNet-50         0.1435         0.6010         0.5375         0.4273         28.82         0.9448           DenseNet         0.9915         0.9955         0.9940         0.9937         0.9843         29.07         0.9556           MISLNet         0.9665         0.9970	Xception	1.0000	1.0000	1.0000	1.0000	45.52	0.9875				
MISLNet PHNet         0.9965         0.9905         0.9950         0.9940         51.28         0.9925           PHNet         1.0000         0.8497         0.9985         0.9494         41.85         0.9753           SRNet         0.8080         0.8855         0.9480         0.8805         50.97         0.9925           ImageCNN         0.9854         0.9935         0.8505         0.9431         53.64         0.9928           CamID CNN         0.92270         0.9357         0.9471         0.9366         48.95         0.9871           Residual Generator [26]           CNNs         StarGAN-v2         StyleGAN         StyleGAN2         Avg.         M.PSNR         M.SSIR           Keeption         0.9820         0.9940         0.9770         0.9843         29.01         0.9498           ResNet-50         0.1435         0.6010         0.5375         0.4273         28.82         0.9440           BenseNet         0.9915         0.9955         0.9940         0.9937         29.72         0.9515           MISLNet         0.9665         0.9470         0.9918         29.82         0.9440           PHNet         0.9665         0.9470         0.9915	ResNet-50	0.7590	0.8770	0.8010	0.8123	35.97	0.9578				
PHNet SRNet         1.0000         0.8497         0.9985         0.9494         41.85         0.9753           SRNet         0.8080         0.8855         0.9480         0.8805         50.97         0.9922           ImageCNN         0.9854         0.9935         0.8505         0.9431         53.64         0.9928           CamID CNN         0.9285         0.9120         0.9870         0.9425         58.10         0.9988           Avg.         0.9270         0.9357         0.9471         0.9366         48.95         0.9871           Residual Ferrator [26]           CNNs         StarGAN-v2         StyleGAN         StyleGAN2         Avg.         M.PSNR         M.SSIR           Xception         0.9820         0.9940         0.9970         0.9843         29.01         0.9488           ResNet-50         0.1435         0.6010         0.5375         0.4273         28.82         0.9448           DenseNet         0.9915         0.9955         0.9940         0.9937         29.72         0.9515           BillsLet         0.9665         0.9970         0.9880         0.9818         29.82         0.9446           PHNet         0.9665         0.9470 <th>DenseNet</th> <th>0.9385</th> <th>0.9770</th> <th>0.9970</th> <th>0.9708</th> <th>54.28</th> <th>0.9997</th>	DenseNet	0.9385	0.9770	0.9970	0.9708	54.28	0.9997				
SRNet         0.8080         0.8855         0.9480         0.8805         50.97         0.9922           ImageCNN         0.9854         0.9935         0.8505         0.9431         53.64         0.9928           Avg         0.9270         0.9357         0.9471         0.9366         48.95         0.9871           Residual Gererator [26]           Residual Gererator [27]           CNNs         StarGAN-v2 StyleGAN StyleGAN2 Avg.         M.PSNR M.SSIR         M.SSIR           Kception         0.9820         0.9940         0.9770         0.9843         29.01         0.9498           ResNet-50         0.1435         0.6010         0.5375         0.4273         28.82         0.9448           DenseNet         0.9915         0.9995         0.9940         0.9937         29.72         0.9515           MISLNet         0.9665         0.9970         0.9880         0.9818         29.27         0.9515           RNet         0.9665         0.9470         0.9915         0.9683         30.21         0.9556           SRNet         0.9605         0.9885         0.9770         0.9733         29.46         0.9474           Image CNN         1.	MISLNet	0.9965	0.9905	0.9950	0.9940	51.28	0.9925				
ImageCNN	PHNet	1.0000	0.8497	0.9985	0.9494	41.85	0.9753				
CamID CNN Avg.         0.9285 0.9270         0.9120 0.9357         0.9870 0.9471         0.9365 0.9871         58.10 0.9871         0.9988 48.95         0.9871 0.9871           CNNs Xception         StarGAN-v2 0.9820         StyleGAN 0.9940         StyleGAN 0.9770         0.9843 0.9843         M_PSNR 29.01         M_SSIR 0.9488           ResNet-50 0 0.1435         0.6010 0.9955         0.9940 0.9940         0.9937 0.9937         29.72 29.72         0.9448 0.9972         0.9448 0.9912         0.9940 0.9937         0.9937 29.72         29.72 0.972         0.9448 0.9446           BINSLNet         0.9605         0.9970         0.9880         0.9818 0.9683         29.82 0.946         0.9440 0.9455           SRNet         0.9665         0.9470         0.9915 0.9985         0.9970 0.9770         0.9753 0.9683         30.21 0.9536         0.9456 0.9466         0.9470 0.9955           CamiD CNN         0.9955 0.8950         0.9990 0.9980         0.9880 0.9730         0.8744 0.9950         0.9550 0.9950           CNNs Ception         StarGAN-v2 0.4235         StyleGAN 0.0005         StyleGAN2 0.6665         Avg. 0.6665         M.PSNR M.PSNR 0.6605         M.PSNR 0.9598         M.PSNR 0.9598           ResNet-50 0.4235         0.8150 0.4235         0.9065 0.9995         0.9997 0.9997         33.11 0.9755 0.9965         0.9997 0.9997	SRNet	0.8080	0.8855	0.9480	0.8805	50.97	0.9922				
Avg.         0.9270         0.9357         0.9471         0.9366         48.95         0.9871           Residual Serierator [26]           Exeridor         0.9820         0.9940         0.9770         0.9843         29.01         0.9498           Xception         0.9820         0.9940         0.9770         0.9843         29.01         0.9498           ResNet-50         0.1435         0.6010         0.5375         0.4273         28.82         0.9448           DenseNet         0.9915         0.9995         0.9940         0.9937         29.72         0.9515           MISLNet         0.9605         0.9970         0.9880         0.9818         29.82         0.9444           PHNet         0.9665         0.9470         0.9915         0.9683         30.21         0.9556           SRNet         0.9605         0.9885         0.9770         0.9753         29.46         0.9474           Image CNN         1.0000         0.0000         1.0000         0.96667         29.21         0.9351           Avg.         0.8750         0.8150         0.9330         0.8744         29.39         0.9506           CNNs         StarGAN-v2         StyleGAN	ImageCNN	0.9854	0.9935	0.8505	0.9431	53.64	0.9928				
Residual Generator   26	CamID CNN	0.9285	0.9120	0.9870	0.9425	58.10	0.9988				
CNNs         StarGAN-v2         StyleGAN         StyleGAN2         Avg.         M.PSNR         M.SSIR           Xception         0.9820         0.9940         0.9770         0.9843         29.01         0.9498           ResNet-50         0.1435         0.6010         0.5375         0.4273         28.82         0.9448           DenseNet         0.9915         0.9955         0.9940         0.9937         29.72         0.9515           MISLNet         0.9605         0.9970         0.9880         0.9818         29.82         0.9446           PHNet         0.9605         0.9870         0.9915         0.9683         30.21         0.9556           SRNet         0.9605         0.9885         0.9770         0.9753         29.46         0.9471           Image CNN         1.0000         0.0000         1.0000         0.6667         29.21         0.9531           CamID CNN         0.9955         0.9995         0.9990         0.9880         28.89         0.9530           Avg.         0.8750         0.8150         0.9330         0.8744         29.39         0.9500           WISLGAN Generator [9]         **** MISLGAN Generator [9]***           CNNs         StarGAN-	Avg.	0.9270	0.9357	0.9471	0.9366	48.95	0.9871				
Xception         0.9820         0.9940         0.9770         0.9843         29.01         0.9498           ResNet-50         0.1435         0.6010         0.5375         0.4273         28.82         0.9448           DenseNet         0.9915         0.9955         0.9940         0.9937         29.72         0.9515           MISLNet         0.9605         0.9970         0.9880         0.9818         29.82         0.9444           PHNet         0.9665         0.9470         0.9915         0.9683         30.21         0.9556           SRNet         0.9665         0.9470         0.9915         0.9683         30.21         0.9556           SRNet         0.9605         0.9885         0.9770         0.9753         29.46         0.9476           CamID CNN         0.9955         0.9995         0.9990         0.9980         28.89         0.9536           Avg.         0.8750         0.8150         0.9330         0.8744         29.39         0.9500           CNNs         StarGAN-v2         StyleGAN StyleGAN2         Avg.         M.PSNR         M.SSIR           Xeeption         1.0000         0.0005         1.0000         0.6665         32.24         0.9598			Residual (	Generator [26]							
ResNet-50         0.1435         0.6010         0.5375         0.4273         28.82         0.9448           DenseNet         0.9915         0.9955         0.9940         0.9937         29.72         0.9515           MISLNet         0.9605         0.9970         0.9880         0.9818         29.82         0.9448           PHNet         0.9665         0.9470         0.9915         0.9683         30.21         0.9556           SRNet         0.9605         0.9885         0.9770         0.9753         29.46         0.9474           Image CNN         1.0000         0.0000         1.0000         0.6667         29.21         0.9531           Avg.         0.8750         0.8150         0.9330         0.8744         29.39         0.9500           CNNs         StarGAN-v2         StyleGAN         StyleGAN         Avg.         M-PSNR         M-SSIR           Xception         1.0000         0.0005         1.0000         0.6668         32.24         0.9598           ResNet-50         0.4235         0.8115         0.7465         0.6605         34.64         0.9635           DenseNet         0.9995         0.9995         0.9999         0.9997         35.11         0.	CNNs	StarGAN-v2	StyleGAN	StyleGAN2	Avg.	M_PSNR	M_SSIM				
DenseNet         0.9915         0.9955         0.9940         0.9937         29.72         0.9515           MISLNet         0.9605         0.9970         0.9880         0.9818         29.82         0.9440           PHNet         0.9605         0.9470         0.9915         0.9683         30.21         0.9558           SRNet         0.9605         0.9885         0.9770         0.9753         29.46         0.9474           Image CNN         1.0000         0.0000         1.0000         0.6667         29.21         0.9531           CamID CNN         0.9955         0.9995         0.9990         0.9980         28.89         0.9536           Avg.         0.8750         0.8150         0.9330         0.8744         29.39         0.9500           TWISLGAN Generator [9]           CNNs         StarGAN-v2         StyleGAN         StyleGAN2         Avg.         M.PSNR         M.SSIR           Xception         1.0000         0.0005         1.0000         0.6668         32.24         0.9598           ResNet-50         0.4235         0.8115         0.7465         0.6605         34.64         0.9635           DenseNet         0.9995         0.9995         0	Xception	0.9820	0.9940	0.9770	0.9843	29.01	0.9498				
MISLNet PHNet         0.9605         0.9970         0.9880         0.9818         29.82         0.9440           PHNet SRNet         0.9665         0.9470         0.9915         0.9683         30.21         0.9556           SRNet         0.9605         0.9885         0.9770         0.9753         29.46         0.9474           Image CNN         1.0000         0.0000         1.0000         0.6667         29.21         0.9531           CamID CNN         0.8750         0.8995         0.9990         0.9800         28.89         0.9536           Avg         0.8750         0.8150         0.9330         0.8744         29.39         0.9500           CNNs         StarGAN-v2         StyleGAN         StyleGAN2         Avg.         M.PSNR         M.SSIP           Xception         1.0000         0.0005         1.0000         0.6668         32.24         0.9598           ResNet-50         0.4235         0.8115         0.7465         0.6605         34.64         0.9635           DenseNet         0.9995         1.0000         0.9995         0.9997         35.11         0.9755           MISLNet         0.9515         0.9965         0.9899         0.9973         34	ResNet-50	0.1435	0.6010	0.5375	0.4273	28.82	0.9448				
PHNet SRNet         0.9665 0.9605         0.9470 0.9885         0.9915 0.9770         0.9683 0.9730         30.21 29.46 29.21         0.9556 0.9474           Image CNN CamiD CNN         1.0000 0.9955         0.0900 0.9995         1.0000 0.9990         0.9880 0.9830         28.89 0.8734         0.9530 29.39         0.9506           Avg.         MISLGAN Generator [9]           CNNs         StarGAN-v2         StyleGAN StyleGAN2         Avg.         M.PSNR M.SSIR Xception         1.0000         0.0005         1.0000         0.6668         32.24         0.9598           ResNet-50         0.4235         0.8115         0.7465         0.6605         34.64         0.9630           DenseNet         0.9995         0.9995         0.9999         0.9997         34.50         0.9660           MISLNet         0.9515         0.9965         0.9899         0.9793         34.84         0.9648           SRNet         0.8915         0.9735         0.9635         0.9428         33.09         0.9548           Image CNN         0.7975         0.7980         0.8205         0.8053         34.36         0.9657	DenseNet	0.9915	0.9955	0.9940	0.9937	29.72	0.9515				
SRNet         0.9605         0.9885         0.9770         0.9753         29.46         0.9474           Image CNN         1.0000         0.0000         1.0000         0.6667         29.21         0.9531           CamID CNN         0.9955         0.9995         0.9990         0.9980         28.89         0.9536           Mrs. or	MISLNet	0.9605	0.9970	0.9880	0.9818	29.82	0.9440				
Image CNN CamID CNN CamID CNN CamID CNN CamID CNN Camid CNN CNN CNN CNN CNN CNN CNN CNN CNN CN	PHNet	0.9665	0.9470	0.9915	0.9683	30.21	0.9556				
CamID CNN Avg.         0.9955 0.8750         0.9995 0.8150         0.9990 0.9330         0.9800 0.8744         28.89 29.39         0.9500 0.9500           CNNs         StarGAN-v2         StyleGAN StyleGAN2         Avg. Avg. Avg.         M-PSNR M-PSNR M-SSIR         M-SSIR 0.9598           ResNet-50         0.4235         0.8115         0.7465         0.6605         34.64         0.9598           DenseNet         0.9995         1.0000         0.9995         0.9997         35.11         0.9755           MISLNet         0.9515         0.9965         0.9989         0.9703         34.50         0.9648           PHNet         0.9925         0.9995         0.9985         0.9968         34.84         0.9648           SRNet         0.8915         0.9735         0.9635         0.9428         33.09         0.9555           Image CNN         0.7975         0.7980         0.8205         0.8053         34.36         0.9657	SRNet	0.9605	0.9885	0.9770	0.9753	29.46	0.9474				
Avg.         0.8750         0.8150         0.9330         0.8744         29.39         0.9500           MISLGAN Generator [9]           CNNs         StarGAN-v2         StyleGAN         StyleGAN2         Avg.         M.PSNR         M.SSIR           Xception         1.0000         0.0005         1.0000         0.6668         32.24         0.9598           ResNet-50         0.4235         0.8115         0.7465         0.6605         34.64         0.9630           DenseNet         0.9995         1.0000         0.9995         0.9997         35.11         0.9755           MISLNet         0.9515         0.9965         0.9899         0.9793         34.50         0.9660           PHNet         0.9925         0.9995         0.9985         0.9968         34.84         0.9648           SRNet         0.8915         0.9735         0.9635         0.9428         33.09         0.9550           Image CNN         0.7975         0.7980         0.8205         0.8053         34.36         0.9657		1.0000	0.0000	1.0000	0.6667		0.9531				
CNNS   StarGAN-v2   StyleGAN   StyleGAN2   Avg.   M.PSNR   M.SSIR	CamID CNN	0.9955	0.9995	0.9990	0.9980	28.89	0.9536				
CNNs         StarGAN-v2         StyleGAN         StyleGAN2         Avg.         M.PSNR         M.SSIR           Xception         1.0000         0.0005         1.0000         0.6668         32.24         0.9598           ResNet-50         0.4235         0.8115         0.7465         0.6605         34.64         0.9630           DenseNet         0.9995         1.0000         0.9995         0.9997         35.11         0.9755           MISLNet         0.9515         0.9965         0.9989         0.9793         34.50         0.9660           PHNet         0.9925         0.9995         0.9985         0.9968         34.84         0.9648           SRNet         0.8915         0.9735         0.9635         0.9428         33.09         0.9555           Image CNN         0.7975         0.7980         0.8205         0.8053         34.36         0.9657	Avg.	0.8750	0.8150	0.9330	0.8744	29.39	0.9500				
Xception         1.0000         0.0005         1.0000         0.6668         32.24         0.9598           ResNet-50         0.4235         0.8115         0.7465         0.6605         34.64         0.9630           DenseNet         0.9995         1.0000         0.9995         0.9997         35.11         0.9755           MISLNet         0.9515         0.9965         0.9899         0.9793         34.50         0.9660           PHNet         0.9925         0.9995         0.9985         0.9968         34.84         0.9648           SRNet         0.8915         0.9735         0.9635         0.9428         33.09         0.9550           Image CNN         0.7975         0.7980         0.8205         0.8053         34.36         0.9657			MISLGAN	Generator [9]	]						
ResNet-50         0.4235         0.8115         0.7465         0.6605         34.64         0.9630           DenseNet         0.9995         1.0000         0.9995         0.9997         35.11         0.9755           MISLNet         0.9515         0.9965         0.9899         0.9793         34.50         0.9660           PHNet         0.9925         0.9995         0.9985         0.9968         34.84         0.9648           SRNet         0.8915         0.9735         0.9635         0.9428         33.09         0.9550           Image CNN         0.7975         0.7980         0.8205         0.8053         34.36         0.9657	CNNs	StarGAN-v2	StyleGAN	StyleGAN2	Avg.	M_PSNR	M_SSIM				
DenseNet         0.9995         1.0000         0.9995         0.9997         35.11         0.9755           MISLNet         0.9515         0.9965         0.9899         0.9793         34.50         0.9666           PHNet         0.9925         0.9995         0.9985         0.9968         34.84         0.9648           SRNet         0.8915         0.9735         0.9635         0.9428         33.09         0.9550           Image CNN         0.7975         0.7980         0.8205         0.8053         34.36         0.9657		1.0000					0.9598				
MISLNet         0.9515         0.9965         0.9899         0.9793         34.50         0.9660           PHNet         0.9925         0.9995         0.9985         0.9968         34.84         0.9648           SRNet         0.8915         0.9735         0.9635         0.9428         33.09         0.9550           Image CNN         0.7975         0.7980         0.8205         0.8053         34.36         0.9657	ResNet-50	0.4235	0.8115	0.7465	0.6605	34.64	0.9630				
PHNet         0.9925         0.9995         0.9985         0.9968         34.84         0.9648           SRNet         0.8915         0.9735         0.9635         0.9428         33.09         0.9550           Image CNN         0.7975         0.7980         0.8205         0.8053         34.36         0.9657		0.9995	1.0000	0.9995	0.9997		0.9755				
SRNet         0.8915         0.9735         0.9635         0.9428         33.09         0.9550           Image CNN         0.7975         0.7980         0.8205         0.8053         34.36         0.9657	MISLNet	0.9515	0.9965	0.9899	0.9793	34.50	0.9660				
Image CNN         0.7975         0.7980         0.8205         0.8053         34.36         0.9657		0.9925	0.9995	0.9985	0.9968		0.9648				
		0.8915	0.9735	0.9635		33.09	0.9550				
Com ID CNN   0.5410   0.2540   0.2720   0.4222   22.20   0.0660		0.7975	0.7980	0.8205	0.8053		0.9657				
Camin Civit 0.3410 0.3340 0.3720 0.4223 33.30 0.9009	CamID CNN	0.5410	0.3540	0.3720	0.4223	33.30	0.9669				
Avg. 0.8246 0.7417 0.8613 0.8092 34.01 0.9646	Avg.	0.8246	0.7417	0.8613	0.8092	34.01	0.9646				

Table 4. Attack success rates and image quality achieved for white box attacks on the Object Dataset.

on allac	ox attacks on the Object Dataset.								
Proposed Adversarial Generator									
CNNs	ProGAN	CycleGAN	StyleGAN	StyleGAN2	BigGAN	GauGAN	Avg.	M_PSNR	M_SSIM
Xception	0.9880	0.9871	0.9995	1.0000	0.9975	0.9992	0.9952	52.59	0.9972
ResNet-50	0.9174	0.8720	0.9910	0.9971	0.9520	0.9848	0.9524	55.41	0.9973
DenseNet	0.8583	0.8432	0.9457	0.9474	0.9350	0.9402	0.9116	50.22	0.9893
MISLNet	0.9437	0.6409	0.9893	0.9954	0.9930	0.9994	0.9270	50.97	0.9925
PHNet	0.9645	0.9477	0.9834	0.9985	0.9890	0.9978	0.9802	51.99	0.9613
SRNet	0.7980	0.5758	0.9577	0.9959	0.7600	0.8846	0.8287	56.41	0.9940
Image CNN	0.6890	0.6644	0.9341	0.9772	0.8540	0.7152	0.8057	55.32	0.9981
CamID CNN	0.8650	0.8470	0.9694	0.9622	0.9445	0.9946	0.9305	52.77	0.9970
Avg.	0.8780	0.7973	0.9713	0.9842	0.9281	0.9395	0.9164	53.21	0.9908
				sidual Generat				•	
CNNs	ProGAN	CycleGAN	StyleGAN	StyleGAN2	BigGAN	GauGAN	Avg.	M_PSNR	M_SSIM
Xception	0.9927	0.9954	0.9983	0.9936	0.9975	1.0000	0.9963	39.73	0.9612
ResNet-50	0.9197	0.9447	0.9376	0.9588	0.9490	0.9670	0.9461	38.51	0.9728
DenseNet	0.9582	0.9242	0.9677	0.9724	0.9585	0.9322	0.9522	37.52	0.9543
MISLNet	0.7800	0.6068	0.7952	0.9644	0.8910	0.9934	0.8353	40.49	0.9875
PHNet	0.9287	0.9758	0.9405	0.9766	0.9745	0.9916	0.9646	40.22	0.9719
SRNet	0.7215	0.6485	0.8590	0.9658	0.8180	0.9110	0.8206	37.36	0.9649
Image CNN	0.6580	0.6114	0.7811	0.9543	0.5905	0.2096	0.6342	38.66	0.9679
CamID CNN	0.6207	0.6121	0.8789	0.9669	0.8860	0.8590	0.8039	39.02	0.9736
Avg.	0.8224	0.7899	0.8949	0.9691	0.8831	0.8580	0.8695	38.94	0.9693
				SLGAN Gener					
CNNs	ProGAN	CycleGAN	StyleGAN	StyleGAN2	BigGAN	GauGAN	Avg.	M_PSNR	M_SSIM
Xception	0.9405	0.9477	0.9666	0.9783	0.9155	0.9414	0.9483	32.09	0.9651
ResNet-50	0.9117	0.8955	0.9025	0.7645	0.9614	0.8720	0.8846	31.50	0.9547
DenseNet	0.9687	0.9227	0.9674	0.9772	0.9300	0.9432	0.9515	31.22	0.8470
MISLNet	0.9905	0.9905	0.9915	0.9880	0.9910	0.9955	0.9912	31.75	0.9602
PHNet	0.8200	0.8465	0.8215	0.8250	0.8305	0.8405	0.8307	31.00	0.9495
SRNet	0.9230	0.8114	0.9719	0.9979	0.9495	0.9896	0.9406	31.68	0.9689
Image CNN	0.7333	0.7205	0.8879	0.9866	0.8000	0.7368	0.8109	33.43	0.8750
CamID CNN	0.6925	0.6636	0.7821	0.9417	0.6995	0.7618	0.7569	31.37	0.9120
Avg.	0.8725	0.8498	0.9114	0.9324	0.8847	0.8851	0.8893	31.76	0.9291

Human Face Dataset Attack Success Rates: Each entry in the left section of Table 3 corresponds to the attack success rate against a particular victim CNN detector. On average, our proposed attack achieved 0.9366 attack success rate on fooling CNN detectors trained to detect GANgenerated images of human faces. Particularly, the proposed attack achieved above 0.90 average attack success rate associated with each GAN method. This means the proposed attack can successfully falsify forensic traces left by StyleGAN, StyleGAN2, and StarGAN-v2. Additionally, the average attack success rates associated with each CNN detector were mostly above 0.94. It means that the proposed

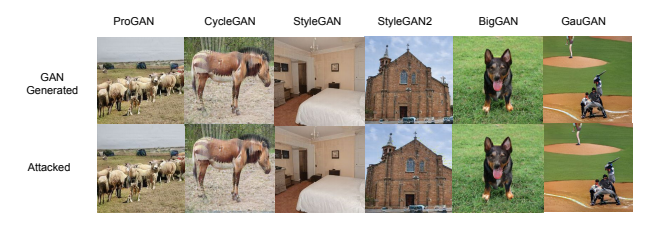


Figure 2. Attacked images produced by our white box attack.

attack can fool each victim CNN detector strongly.

Object Dataset Attack Success Rates: Each entry in the left section of Table 4 corresponds to the attack success rate achieved on the object dataset against a particular victim CNN detector. On average, the proposed attack achieved 0.9164 attack success rate on fooling CNN detectors trained to detect GAN-generated images of objects. The average attack success rates associated with each GAN method are mostly above 0.9000. The results showed that the proposed attack can falsify forensic traces left by a variety of GAN methods. The average attack success rates associated with each CNN detector are mostly above 0.9000. These results showed the proposed attack can successfully fool individual victim CNN detector strongly. We note that for attacks on the object dataset, the proposed attacks were trained only using ProGAN generated images. However, the proposed attack can still fool the CNN detectors when applying the attack on generated images produced by other GAN methods. It means that the proposed attack can remove forensic traces left by unseen GAN methods.

Visual Quality: The right sections of Table 3 and Table 4 show the evaluation of the image quality of attacked images produced by the proposed attack. On the human face dataset, the average mean PSNR is 48.95 and the average mean PSNR is 53.21 and the average mean SSIM 0.9908. The results mean the attacked images produced by our proposed attack can maintain very high visual quality.

We present attacked images produced by the proposed attack in Figure 2. These attacked images were created using the anti-forensic generator trained against ResNet-50. Visually comparing the GAN-generated images to the attacked images, we can see that there is no visible difference between the two. This demonstrates that our attack will not leave behind visual cues and it will not alter the content of the attacked image in an undesirable manner.

Comparing with Other Generators: We compared the performance of the proposed anti-forensic generator with two previous work [26, 9] that also used GAN-based generators to falsify forensic traces of images.

In terms of attack success rates, Table 3 shows that on the human face dataset, our proposed generator achieved 6% higher on average than the residual generator [26], and

Table 5. Attack success rates and image quality achieved for zero knowledge attacks on the Human Face Dataset.

CNNs	StarGAN-v2	StyleGAN	StyleGAN2	Avg.	M_PSNR	M_SSIM
Xception	0.7855	0.9565	0.9900	0.9107	37.93	0.9766
ResNet-50	0.0695	0.3795	0.2815	0.2435	42.90	0.9765
DenseNet	0.8345	0.8325	0.9520	0.8730	38.79	0.9480
MISLNet	0.1250	0.2340	0.8350	0.3980	38.14	0.9742
PHNet	0.9925	0.7625	0.9935	0.9162	41.69	0.9704
SRNet	0.8495	0.8675	0.9465	0.8878	40.16	0.9709
Image CNN	0.8360	0.9595	0.8065	0.8673	41.27	0.9590
CamID CNN	0.7990	0.9480	0.9880	0.9117	42.77	0.9703
Avg.	0.6614	0.7425	0.8491	0.7510	40.46	0.9682

Table 6. Attack success rates and image quality achieved for zero knowledge attacks on the Object Dataset.

	_			J					
CNNs	ProGAN	CycleGAN	StyleGAN	StyleGAN2	BigGAN	GauGAN	Avg.	M_PSNR	M_SSIM
Xception	0.9215	0.9568	0.9811	0.9986	0.9525	0.9684	0.9663	39.95	0.9510
ResNet-50	0.7022	0.7742	0.7798	0.7816	0.8990	0.8902	0.8045	41.75	0.9628
DenseNet	0.9692	0.9508	0.9712	0.8922	0.9540	0.9740	0.9519	40.46	0.9214
MISLNet	0.1163	0.1318	0.1264	0.1325	0.3035	0.6920	0.2504	41.39	0.9353
PHNet	0.9525	0.9652	0.9796	0.9959	0.9669	0.9888	0.9748	42.18	0.9417
SRNet	0.0223	0.0000	0.2483	0.2359	0.0010	0.0020	0.0849	39.95	0.9510
Image CNN	0.6515	0.6136	0.8462	0.9238	0.4840	0.1036	0.6038	41.03	0.9653
CamID CNN	0.9885	0.9561	0.9997	0.9990	1.0000	1.0000	0.9906	43.43	0.9361
Avg.	0.6655	0.6686	0.7415	0.7449	0.6961	0.7024	0.7030	41.27	0.9456

12% higher than the MISLGAN generator. Table 4 shows that on the object dataset, our proposed generator achieved 4.5% higher on average than the residual generator [26], and 12% higher than the MISLGAN generator.

In terms of image quality, on both datasets our proposed attack dramatically outperforms the other two generators. On the human face dataset, the proposed generator achieved 20 dB higher mean PSNR than the residual generator and 15 dB higher mean PSNR than the MISLGAN generator, 3% higher mean SSIM than the residual generator and 2.5% higher mean SSIM than the MISLGAN generator. On the object dataset, the proposed generator achieved 14 dB higher mean PSNR than the residual generator and 21 dB higher mean PSNR than the MISLGAN generator, 2% higher mean SSIM than the residual generator and 6% higher mean SSIM than the MISLGAN generator.

To summarize, in the white-box scenario, we demonstrated that our proposed attack can successfully fool victim CNN detectors on both the human face dataset and the object dataset. The attacked images produced by our attack have high visual quality. We also demonstrated that our proposed attack outperformed previous works.

# 5.2. Results for Zero Knowledge Attack

Table 5 shows the evaluation of the proposed attack achieved on the human face dataset, and Table 6 shows the evaluation of the propose attack achieved on the object dataset. The attack success rates achieved against the victim CNN detectors are shown in the left sections of the tables. The evaluation of the visual quality of the attacked images are shown in the right sections of the tables.

Human Face Dataset Attack Success Rates: Each entry in the left section of Table 5 corresponds to the attack success rate against a particular victim CNN detector. On average, the proposed attack achieved 0.7510 attack success rate on fooling CNN detectors trained to detect GAN-

generated images of human faces. While the average attack success rate decreased 15% comparing with the white-box scenario, it was mainly because of low attack success rates against ResNet-50 and MISLNet. We still achieved high attack success rates for the other six CNN detectors.

Object Dataset Attack Success Rates: Each entry in the left section of Table 6 corresponds to the attack success rate against a particular victim CNN detector. On average, the proposed attack achieved 0.7030 attack success rate on fooling CNN detectors trained to detect GAN-generated images of objects. We note that the drop on the average attack success rate comparing to the white-box scenario was mainly caused by SRNet and MISLNet. We still achieved high attack success rates for the other six CNN detectors.

**Interpretation of the Results**: The attack success rates achieved on both datasets demonstrate that the proposed attack can transfer to fool CNN detectors even when the attacker has zero knowledge about the CNN detectors. The results are important because it shows that our attack can be launched in a realistic scenario. While the results are not perfect, particularly in the attacks against ResNet-50 and MISLNet on the human faces dataset and the attacks against MISLNet and SRNet on the object dataset, the results still strongly show that the proposed attack can pose enough threat, since it worked great on the majority of the testing cases. For example, the attack success rates against Xception are uniformly high (over 0.9000) on both datasets. One possible explanation for the low attack success rates in some cases could be that forensic traces learned by these victim CNN detectors are not located in the same feature space as the ensemble of CNN detectors used to train the attack. However, we think it may provide some insights for the investigators and researchers developing defense strategies against similar types of attack.

Visual Quality: The right sections of Table 5 and Table 6 show the evaluation of the image quality of attacked images produced by the proposed attack. On the human face dataset, the average mean PSNR is 40.46 and the average mean SSIM is 0.9682. On the object database, the average mean PSNR is 41.27 and the average mean SSIM is 0.9456. These results show that the attacked images produced by our proposed attack maintain high visual quality.

We present attacked images of human faces produced by the proposed attack in Figure 3. These attacked images were created using anti-forensic generator trained against Xception. Visually comparing the GAN-generated images to the attacked images, we can see that there is no visible difference between the two. This demonstrates that our attack will not leave behind visual cues and it will not alter the content of the attacked image in an undesirable manner.



Figure 3. Attacked images produced by zero knowledge attack.

#### 5.3. Invariance to Detection Block Alignment

When confronted with large GAN-generated images, synthetic image detection CNNs typically analyze either one or several smaller blocks of the image. Many existing adversarial attacks either assume that all images are the same size as the victim classifier's input, or that the location of the block (or blocks) analyzed by the victim classifier is know to the attacker. By contrast, our proposed attack requires no advanced knowledge of the block or blocks that the victim classifier will analyze. Since our attack is deployed via a fully convolution generator, it can be used to attack an entire image of arbitrary size. Any block analyzed by the victim CNN will contain falsified forensic traces.

We demonstrated that our proposed attack is agnostic to blocking synchronization with the victim CNN by evaluating the proposed attack on large scale images (i.e bigger than the input size of the victim classifier). Specifically, this can be seen by examining our attacks ASR using Style-GAN and StyleGAN2 generated images of human faces as shown in Table 3, since they are of size  $1024 \times 1024$ . Our anti-forensic generator was trained using  $256 \times 256$  in the attacker's training set, then deployed on the full sized  $1024 \times 1024$  images in the evaluation set. The victim CNNs analyzed these images by randomly cropping a  $256 \times 256$ image block for analysis. The high attack success rates achieved on attacking StyleGAN and StyleGAN2 generated images of human faces demonstrates that a randomly selected image patch from the attacked image can still fool the CNN detectors.

# 6. Conclusion

In this paper, we proposed a new attack to fool GAN-generated image detectors. Our attack uses an adversarially trained generater to synthesize forensic traces that these detectors associate with 'real' images. We proposed training protocols to produce both white box as well as zero-knowledge attacks. The latter protocol, which is based on training against an ensemble of classifiers, enables our attack to achieve transferability to unseen victim classifiers. Through a series of experiments, we demonstrated that our attack does not create perceptible distortions in attacked images, and can fool eight different GAN-generated image detectors.

### References

- [1] Mauro Barni, Kassem Kallas, Ehsan Nowroozi, and Benedetta Tondi. On the transferability of adversarial examples against cnn-based image forensics. 2019 IEEE International Conference on Acoustics, Speech and Signal Processing, pages 8286–8290, 2019. 1, 2
- [2] Mauro Barni, Matthew C Stamm, and Benedetta Tondi. Adversarial multimedia forensics: Overview and challenges ahead. In 2018 26th European Signal Processing Conference (EUSIPCO), pages 962–966. IEEE, 2018. 1, 2
- [3] Belhassen Bayar and Matthew C Stamm. Constrained convolutional neural networks: A new approach towards general purpose image manipulation detection. *IEEE Transactions on Information Forensics and Security*, 13(11):2691–2706, 2018. 5
- [4] Mehdi Boroumand, Mo Chen, and Jessica Fridrich. Deep residual network for steganalysis of digital images. *IEEE Transactions on Information Forensics and Security*, 14(5):1181–1193, 2018. 5
- [5] Mehdi Boroumand and Jessica Fridrich. Deep learning for detecting processing history of images. *Electronic Imaging*, 2018(7):213–1, 2018. 5
- [6] Andrew Brock, Jeff Donahue, and Karen Simonyan. Large scale gan training for high fidelity natural image synthesis. *arXiv preprint arXiv:1809.11096*, 2018. 1, 5
- [7] Nicholas Carlini and Hany Farid. Evading deepfake-image detectors with white-and black-box attacks. In *Proceedings* of the IEEE/CVF Conference on Computer Vision and Pattern Recognition Workshops, pages 658–659, 2020. 1, 2
- [8] N. Carlini and D. Wagner. Towards evaluating the robustness of neural networks. In 2017 IEEE Symposium on Security and Privacy, pages 39–57, May 2017. 1, 2
- [9] Chen Chen, Xinwei Zhao, and Matthew C Stamm. Misl-gan: an anti-forensic camera model falsification framework using a generative adversarial network. In 2018 25th IEEE International Conference on Image Processing (ICIP), pages 535–539. IEEE, 2018. 2, 6, 7
- [10] Yunjey Choi, Minje Choi, Munyoung Kim, Jung-Woo Ha, Sunghun Kim, and Jaegul Choo. Stargan: Unified generative adversarial networks for multi-domain image-to-image translation. In *Proceedings of the IEEE Conference on Com*puter Vision and Pattern Recognition, 2018. 1
- [11] Yunjey Choi, Youngjung Uh, Jaejun Yoo, and Jung-Woo Ha. Pre-trained stargan-v2. https://github.com/clovaai/stargan-v2, 2019. 4
- [12] Yunjey Choi, Youngjung Uh, Jaejun Yoo, and Jung-Woo Ha. Stargan v2: Diverse image synthesis for multiple domains. In *Proceedings of the IEEE Conference on Computer Vision and Pattern Recognition*, 2020. 1, 4
- [13] François Chollet. Xception: Deep learning with depthwise separable convolutions. In *Proceedings of the IEEE con*ference on computer vision and pattern recognition, pages 1251–1258, 2017. 5
- [14] Davide Cozzolino, Justus Thies, Andreas Rössler, Matthias Nießner, and Luisa Verdoliva. Spoc: Spoofing camera fingerprints. arXiv preprint arXiv:1911.12069, 2019. 2

- [15] Davide Cozzolino, Justus Thies, Andreas Rössler, Christian Riess, Matthias Nießner, and Luisa Verdoliva. Forensictransfer: Weakly-supervised domain adaptation for forgery detection. arXiv preprint arXiv:1812.02510, 2018. 1, 2
- [16] Xavier Glorot and Yoshua Bengio. Understanding the difficulty of training deep feedforward neural networks. In Yee Whye Teh and Mike Titterington, editors, *Proceedings of the Thirteenth International Conference on Artificial Intelligence and Statistics*, volume 9 of *Proceedings of Machine Learning Research*, pages 249–256, Chia Laguna Resort, Sardinia, Italy, 13–15 May 2010. PMLR. 5
- [17] Ian Goodfellow, Jean Pouget-Abadie, Mehdi Mirza, Bing Xu, David Warde-Farley, Sherjil Ozair, Aaron Courville, and Yoshua Bengio. Generative adversarial nets. In Advances in neural information processing systems, pages 2672–2680, 2014. 1
- [18] Ian J Goodfellow, Jonathon Shlens, and Christian Szegedy. Explaining and harnessing adversarial examples. arXiv preprint arXiv:1412.6572, 2014. 1, 2
- [19] D. Guera, Y. Wang, L. Bondi, P. Bestagini, S. Tubaro, and E. J. Delp. A counter-forensic method for cnn-based camera model identification. In *Computer Vision and Pattern Recognition Workshops (CVPRW)*, pages 1840–1847. IEEE, July 2017. 1, 2
- [20] Kaiming He, Xiangyu Zhang, Shaoqing Ren, and Jian Sun. Deep residual learning for image recognition. In *Proceedings of the IEEE Conference on Computer Vision and Pattern Recognition (CVPR)*, June 2016. 5
- [21] Gao Huang, Zhuang Liu, Laurens Van Der Maaten, and Kilian Q Weinberger. Densely connected convolutional networks. In *Proceedings of the IEEE conference on computer vision and pattern recognition*, pages 4700–4708, 2017. 5
- [22] Andrew Ilyas, Shibani Santurkar, Dimitris Tsipras, Logan Engstrom, Brandon Tran, and Aleksander Madry. Adversarial examples are not bugs, they are features, 2019. 2
- [23] Tero Karras, Timo Aila, Samuli Laine, and Jaakko Lehtinen. Progressive growing of gans for improved quality, stability, and variation. arXiv preprint arXiv:1710.10196, 2017. 1, 4,
- [24] Tero Karras, Samuli Laine, and Timo Aila. A style-based generator architecture for generative adversarial networks. In Proceedings of the IEEE/CVF Conference on Computer Vision and Pattern Recognition, pages 4401–4410, 2019. 1, 4,
- [25] Tero Karras, Samuli Laine, Miika Aittala, Janne Hellsten, Jaakko Lehtinen, and Timo Aila. Analyzing and improving the image quality of StyleGAN. In *Proc. CVPR*, 2020. 1, 4,
- [26] Dongkyu Kim, Han-Ul Jang, Seung-Min Mun, Sunghee Choi, and Heung-Kyu Lee. Median filtered image restoration and anti-forensics using adversarial networks. *IEEE Signal Processing Letters*, 25(2):278–282, 2017. 2, 6, 7
- [27] Alexey Kurakin, Ian Goodfellow, Samy Bengio, et al. Adversarial examples in the physical world, 2016. 1, 2
- [28] Nvidia Research Lab. Public database of stylegan. https://github.com/NVlabs/stylegan, 2019. 4
- [29] Nvidia Research Lab. Public database of stylegan2. https://github.com/NVlabs/stylegan2, 2019. 4

- [30] Aleksander Madry, Aleksandar Makelov, Ludwig Schmidt, Dimitris Tsipras, and Adrian Vladu. Towards deep learning models resistant to adversarial attacks. arXiv preprint arXiv:1706.06083, 2017. 1, 2
- [31] F. Marra, D. Gragnaniello, D. Cozzolino, and L. Verdoliva. Detection of gan-generated fake images over social networks. In 2018 IEEE Conference on Multimedia Information Processing and Retrieval (MIPR), pages 384–389, 2018.
- [32] F. Marra, D. Gragnaniello, L. Verdoliva, and G. Poggi. Do gans leave artificial fingerprints? In 2019 IEEE Conference on Multimedia Information Processing and Retrieval (MIPR), pages 506–511, 2019. 1, 2
- [33] F. Marra, C. Saltori, G. Boato, and L. Verdoliva. Incremental learning for the detection and classification of gan-generated images. In 2019 IEEE International Workshop on Information Forensics and Security (WIFS), pages 1–6, 2019.
- [34] Scott McCloskey and Michael Albright. Detecting gangenerated imagery using color cues. *arXiv preprint arXiv:1812.08247*, 2018. 1, 2
- [35] Vinod Nair and Geoffrey E Hinton. Rectified linear units improve restricted boltzmann machines. In *Proceedings of the 27th international conference on machine learning (ICML-10)*, pages 807–814, 2010. 3
- [36] Lakshmanan Nataraj, Tajuddin Manhar Mohammed, BS Manjunath, Shivkumar Chandrasekaran, Arjuna Flenner, Jawadul H Bappy, and Amit K Roy-Chowdhury. Detecting gan generated fake images using co-occurrence matrices. *Electronic Imaging*, 2019(5):532–1, 2019. 1, 2
- [37] Nicolas Papernot, Patrick McDaniel, Somesh Jha, Matt Fredrikson, Z Berkay Celik, and Ananthram Swami. The limitations of deep learning in adversarial settings. In 2016 IEEE European symposium on security and privacy (EuroS&P), pages 372–387. IEEE, 2016. 1, 2
- [38] Taesung Park, Ming-Yu Liu, Ting-Chun Wang, and Jun-Yan Zhu. Gaugan: semantic image synthesis with spatially adaptive normalization. In *ACM SIGGRAPH 2019 Real-Time Live!*, pages 1–1. 2019. 1, 5
- [39] Christian Szegedy, Wojciech Zaremba, Ilya Sutskever, Joan Bruna, Dumitru Erhan, Ian Goodfellow, and Rob Fergus. Intriguing properties of neural networks, 2014. 1, 2
- [40] A. Tuama, F. Comby, and M. Chaumont. Camera model identification with the use of deep convolutional neural networks. In *International Workshop on Information Forensics and Security (WIFS)*, pages 1–6. IEEE, Dec 2016. 5
- [41] Sheng-Yu Wang, Oliver Wang, Richard Zhang, Andrew Owens, and Alexei A Efros. Cnn-generated images are surprisingly easy to spot... for now. In *Proceedings of the IEEE/CVF Conference on Computer Vision and Pattern Recognition*, pages 8695–8704, 2020. 1, 2, 4
- [42] Fisher Yu, Ari Seff, Yinda Zhang, Shuran Song, Thomas Funkhouser, and Jianxiong Xiao. Lsun: Construction of a large-scale image dataset using deep learning with humans in the loop, 2016. 4
- [43] N. Yu, L. Davis, and M. Fritz. Attributing fake images to gans: Learning and analyzing gan fingerprints. In 2019 IEEE/CVF International Conference on Computer Vision (ICCV), pages 7555–7565, 2019. 1, 2

- [44] Xiaoyong Yuan, Pan He, Qile Zhu, and Xiaolin Li. Adversarial examples: Attacks and defenses for deep learning. IEEE transactions on neural networks and learning systems, 30(9):2805–2824, 2019. 2
- [45] Yifeng Zhan, Yifang Chen, Qiong Zhang, and Xiangui Kang. Image forensics based on transfer learning and convolutional neural network. In *Proceedings of the 5th ACM Workshop* on Information Hiding and Multimedia Security, pages 165– 170, 2017. 5
- [46] Xu Zhang, Svebor Karaman, and Shih-Fu Chang. Detecting and simulating artifacts in gan fake images. In 2019 IEEE International Workshop on Information Forensics and Security (WIFS), pages 1–6. IEEE, 2019. 1, 2
- [47] Xinwei Zhao and Matthew C Stamm. The effect of class definitions on the transferability of adversarial attacks against forensic cnns. *Electronic Imaging*, 2020(4):119–1, 2020. 1,
- [48] Jun-Yan Zhu, Taesung Park, Phillip Isola, and Alexei A Efros. Unpaired image-to-image translation using cycleconsistent adversarial networks. In *Proceedings of the IEEE* international conference on computer vision, pages 2223– 2232, 2017. 5